# Insertion mutation in Tnfrsf11a causes a Paget's disease-like phenotype in heterozygous mice and osteopetrosis in homozygous mice

HOLOGIC®
The Science of Sure

# Powerful images.
# **Clear answers.**

Manage Patient's concerns about Atypical Femur Fracture*

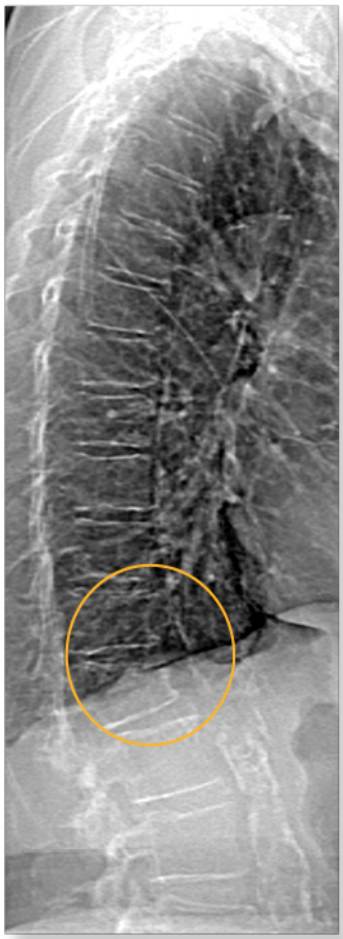

Vertebral Fracture Assessment – a critical part of a complete fracture risk assessment

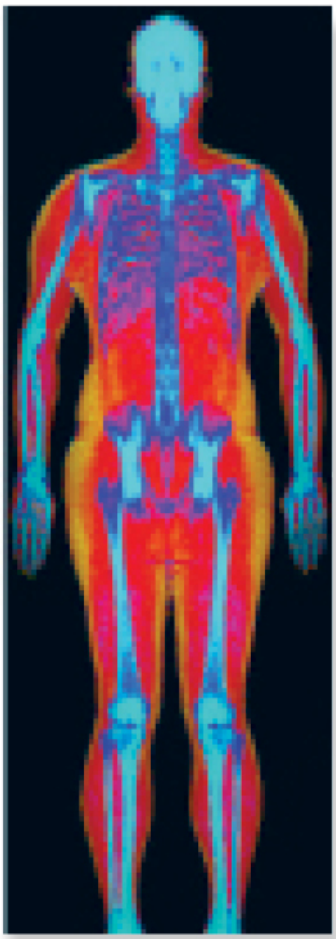

Advanced Body Composition® Assessment – the power to see what's inside

**Contact your Hologic rep today at BSHSalesSupportUS@hologic.com**



*Incomplete Atypical Femur Fractures imaged with a Hologic densitometer, courtesy of Prof. Cheung, University of Toronto



**www.hologic.com | dxaperformance.com | 1.800.442.9892**

# Insertion mutation in *Tnfrsf11a* causes a Paget's disease-like phenotype in heterozygous mice and osteopetrosis in homozygous mice

Nerea Alonso,[1] Sachin Wani,[1] Lorraine Rose,[1,2] Rob J van't Hof,[1,3] Stuart H Ralston,[1] and Omar M E Albagha[1,4]

**Author affiliations**

[1]Rheumatology and Bone Disease Unit, Centre for Genomic and Experimental Medicine, Institute of Genetics and Molecular Medicine, University of Edinburgh, Edinburgh, UK

[2]MRC Human Genetics Unit, MRC IGMM, University of Edinburgh, Edinburgh, UK

[3]Institute of Aging and Chronic Disease, University of Liverpool, Liverpool, UK

[4]College of Health and Life Sciences, Hamad Bin Khalifa University, Doha, Qatar

**Address correspondence to:** Omar M E Albagha or Stuart H Ralston

Rheumatology and Bone Disease Unit,

Centre for Genomic and Experimental Medicine,

University of Edinburgh,

Crewe Road,

Edinburgh EH4 2XU

United Kingdom

Email addresses: omar.albagha@ed.ac.uk, stuart.ralston@ed.ac.uk

Tel: +44 131 651 8727

**Running title:** RANK 75dup27 model for PDB

This manuscript includes Supplemental Information.

This article has been accepted for publication and undergone full peer review but has not been through the copyediting, typesetting, pagination and proofreading process which may lead to differences between this version and the Version of Record. Please cite this article as doi: 10.1002/jbmr.4288

**Disclosure**

Prof S H Ralston holds a grant from the European Commission and has received research funding from Amgen, Eli Lilly, Novartis, and Pfizer unrelated to the submitted work. The other authors have no conflicts of interest to declare.

**Abstract**

Early onset familial Paget's disease of bone (EoPDB), familial expansile osteolysis and expansile skeletal hyperphosphatasia are related disorders caused by insertion mutations in exon 1 of the *TNFRSF11A* gene which encodes receptor activator of nuclear factor kappa B (RANK) protein. To understand the mechanisms underlying these disorders, we developed a mouse model carrying the 75dup27 mutation which causes EoPDB.

Mice heterozygous for the mutation (*Tnfrsf11a*$^{75dup27/-}$) developed a PDB-like disorder with focal osteolytic lesions in the hind limbs with increasing age. Treatment of these mice with zoledronic acid completely prevented the development of lesions. Studies *in vitro* showed that RANKL-induced osteoclast formation and signaling was impaired in bone marrow cells from *Tnfrsf11a*$^{75dup27/-}$ animals, but that osteoclast survival was increased independent of RANKL stimulation. Surprisingly, *Tnfrsf11a*$^{75dup27/75dup27}$ homozygotes had osteopetrosis at birth, with complete absence of osteoclasts. Bone marrow cells from these mice failed to form osteoclasts in response to RANKL and M-CSF stimulation. This intriguing study has shown that in heterozygous form, the 75dup27 mutation causes focal osteolytic lesions *in vivo* reminiscent of the human disorder and extends osteoclast survival independently of RANKL signaling. In homozygous form however, the mutation causes osteopetrosis due to failure of osteoclast formation and insensitivity to RANKL stimulation.

**Keywords**

Paget's disease of bone, RANK, 75dup27, mouse model, osteoclast

## Introduction

Early onset Paget's disease of bone (EoPDB) is a rare condition which has phenotypic overlap with both classical PDB and familial expansile osteolysis [1-3]. It is caused by a heterozygous 27-bp duplication in the signal peptide of *TNFRSF11A* gene (75dup27), leading to insertion of nine amino acids in the RANK signal peptide. It belongs to a group of related focal osteolytic disorders with distinct but overlapping features in which various insertion mutations occur in exon 1 of *TNFRSF11A* causing duplications of between five and nine amino acids in the RANK signal peptide (reviewed in [4]). Previous *in vitro* studies have shown that the causal mutations prevent cleavage of the RANK signal peptide, causing the mutant RANK molecules to accumulate in the Golgi apparatus, impairing its ability to translocate to the cell surface [3,5,6]. This, in turn, has been shown to lead to defective RANKL signaling indicating that these are loss-of-function mutations that impair RANKL induced osteoclastogenesis [5,7]. There remains a conundrum of exactly how loss of function mutations in *TNFRSF11A* can cause an osteolytic disorder *in vivo*. In order to investigate this, we generated a mouse model of the 75dup27 insertion, confirming that this is a loss-of function mutation for RANKL-induced osteoclastogenesis in homozygous form, but is a gain of function mutation in heterozygous due to non-classical activation of NF-κB signaling.

## Materials and Methods

*Generation of the Tnfrsf11a$^{75dup27/75dup27}$ mouse model*

Mice with the *75dup27* mutation were generated by gene targeting in embryonic stem cells according to classical techniques. The targeting construct was created by generating a 4.7 kb fragment by PCR from genomic DNA encompassing exon 1 of the mouse *Tnfrsf11a* gene and surrounding sequences. The 27bp insertion mutation was inserted in the first exon (Suppl Figure S1) by site-directed mutagenesis (Stratagene), followed by cloning a floxed neomycin cassette as a positive selection marker, a 2-kb 3' homology region, and diphtheria toxin A (DTA) cassette as a negative selection marker. Supplementary figure S2A shows schematic representation of the targeting construct. The targeting construct was electroporated into 129/Ola embryonic stem cells (ES). Following selection by culturing the ES cells in neomycin, three positive clones were identified, and fidelity of the targeting event was confirmed by southern blotting with probes at the 5' and 3' ends (Suppl. Fig. S2B). Targeted ES cells were injected into C57BL/6 blastocysts to generate chimeric animals. The neomycin cassette was excised by crossing male chimeras with a CMV-Cre recombinase expressing C57BL/6 female.

Presence of the 27bp-insertion mutation was confirmed by DNA sequencing (Suppl. Figure S2C). The resulting C57BL/6-129Ola mixed-background animals were backcrossed into C57BL/6 for 10 generations and complete backcross was confirmed using Illumina mouse medium-density linkage panel following the manufacturer's recommended protocol (Illumina Inc, USA). All mice were housed in a standard animal facility with free access to food (pelleted RM1; SDS diets, UK) and water. All experiments on mice were performed according to institutional and UK regulations.

*Osteoclast cultures*

Bone marrow was flushed from long bones of 3-4-month-old mice of each genotype and cultured in α-MEM supplemented with 10% fetal calf serum, penicillin/streptomycin, glutamine and MCSF (100 ng/mL) for 48 hours. The culture medium containing non-adherent cells was removed and adherent cells, containing MCSF-dependent osteoclast precursors were removed by trypsinization and plated at a density of $10^4$ cells/well in 96-well plates with 150 µl of culture medium and MCSF at a concentration of 25 ng/mL and different concentrations of RANKL until osteoclasts were formed (4-5 days). At the end of the culture period the medium was removed and the cells were fixed with 4% formaldehyde in PBS and stained for TRAcP [8]. Osteoclasts, defined as TRAcP+ cells with 3 or more nuclei, were counted using a 10x-objective lens on a bright field microscope. Osteoclasts carrying more than 5 nuclei were counted separately.

*Osteoclast survival*

Osteoclasts were generated from bone marrow cells as described above and after 4-5 days in culture RANKL was withdrawn and cultures continued for periods of up to 42 hours. The cultures were stopped at the indicated time points and cells were fixed in 4% formaldehyde in PBS. Staining for osteoclasts was performed as described above.

*Western blot*

The cells were washed in 1 ml of ice-cold PBS and lysed in radioimmunoprecipitation assay (RIPA) buffer. Protein quantification was performed using the Pierce BCA protein assay kit (Life Technologies). Protein lysates were mixed with the appropriate volume of 5X sample loading protein buffer (10% SDS, 500mM DTT, 50% Glycerol, 250mM Tris-HCL and 0.5% bromophenol blue dye, PH 6.8) and denatured at 95□ C on a dry bath for 3-5 min and 60-70 µg loaded into pre-cast acrylamide gels (Bio Rad). Band separation was performed by electrophoresis at 200V for 35-45 min and proteins were transferred to a nylon membrane at 60 mA for 2-3 h. c-Fos, ERK 1/2 (Thr202/Tyr204 p44/p42 MAPK), Ser32 IκB-α,

Thr180/Tyr182 p38 MAPK, as well as their phosphorylated counterparts were detected using rabbit polyclonal antibodies (Suppl Table S1). β-Actin or HPRT was used for normalization and detected using rabbit polyclonal antibody (Suppl Table S1). Horseradish peroxidase-conjugated anti-rabbit secondary antibodies were used to visualize results using Supersignal chemiluminescence kit from Life Technologies in a Syngene Genegnome bioimaging system (Fisher Scientific). Intensities of bands were quantified using Image Studio Lite Ver 3.1 software.

*NF-κB luciferase reporter assay*

MCSF-dependent macrophages were generated from mice as described above and seeded at a density of 1 x $10^6$ cells and cultured in complete α-MEM medium for 24 hours. Subsequently, the cells were transduced with a lentiviral NF-kB luciferase reporter (NF-κB Cignal lenti luciferase reporter assay from SA Bioscience) at a multiplicity of infection (MOI) of 3 in 3ml serum free αMEM media for 5 hrs. An additional 3ml of standard α-MEM was then added to each flask and the cultures were incubated for two days followed by selection for another 48hrs using Puromycin (5μg/ml). The cells were then harvested, plated at $10^4$ cells/well in 96 well plate and cultured in complete α-MEM for 24hrs. Luciferase activity was measured with a SteadyGlo-luciferase reporter assay system (Promega) at the indicated time points following RANKL stimulation (100ng/ml) until osteoclasts were formed, as well as 24 and 48 hrs. post RANKL withdrawal using a Bio-Tek Synergy HT plate reader.

*Measurement of biochemical markers*

Serum levels of P1NP, CTX-I (Immunodiagnostic Systems, UK) and RANKL (ThermoFisher Scientific, UK) were measures using enzyme-linked immunosorbent assay by following the manufacturer's protocol.

*Bone micro-computed tomography (Micro CT) analysis*

MicroCT analysis was performed using a Skyscan 1172 system (Bruker, Belgium). The hind limbs of animals were dissected free of soft tissue, fixed in 4% formaldehyde in PBS, and tibial metaphysis and diaphysis were scanned *ex vivo* at a resolution of 5 μm (60 kV, 167 μA, using a 0.5 mm aluminum filter and a rotation step size of 0.3°). Image reconstruction was performed using the Skyscan NRecon package and trabecular and cortical bone parameters were measured using Skyscan CTAn software as described previously [(9)]. Briefly, trabecular bone parameters were measured in a stack of 200 slices immediately distal from the growth plate and, for cortical bone parameters, in 100 slices at the mid shaft of the femur.

*Semiquantitative analysis of osteolytic lesions*

The presence and numbers of osteolytic lesions were assessed on MicroCT images of the hind limbs. Bone lesions were analyzed using a semi-quantitative 3-point scoring system to grade the lesions based on the size and number of lesions observed. Each animal was given a total lesion score based on the sum of scores generated from the left and right hind limbs.

*Bone histology and histomorphometry*

Histological analysis was performed as described previously [12]. After dissection, hind limbs were fixed for 24 h in 4% buffered formalin and stored in 70% ethanol. The samples were embedded in methyl methacrylate and sections were cut using a tungsten steel knife. Bone sections were stained for TRAcP to visualize osteoclasts and counterstained with Aniline Blue. Cartilage matrix was visualized using Safranin O staining and Fast green as a counterstain. To achieve imaging of entire sections, image fields were stitched together using Microsoft Ice software. Histomorphometry was performed using custom software based on Image J [10] and followed standardized nomenclature and recommendations [11].

*Bisphosphonate therapy*

Heterozygous *Tnfrsf11a*$^{75dup27/-}$ female mice were treated with zoledronic acid at a dose of 85 μg/kg (n = 8) or vehicle (PBS; n=8) between 4 months and 12 months of age by subcutaneous injection every 2 months. The experiment was terminated by culling the mice at 15 months of age, the limbs recovered and analyzed for the presence of bone lesions by microCT and histological analysis.

*Statistical analysis*

Differences between groups were assessed by unpaired Student's T-test using SPSS for Windows version 19. A p-value $< 0.05$ was considered statistically significant. Data are presented as box and whiskers plots showing all data points, the interquartile range, the minimum and maximum values.

*Ethical considerations*

Ethical approval for the experiments was obtained from the Animal Welfare and the Ethical Review Body of the University of Edinburgh and the experiments were conducted according to the UK Animals Act of 1986 (Scientific Procedures).

## Results

*Phenotype of homozygous Tnfrsf11a*$^{75dup27/75dup27}$ *mice*

Mice that were homozygous for the 27-bp insertion of RANK (*Tnfrsf11a*$^{75dup27/75dup27}$) were viable but were smaller than their wild type littermates. By the time of weaning, *Tnfrsf11a*$^{75dup27/75dup27}$ mice lacked incisors, and they were fed a soft food diet. They also had reduced survival; 31% (5 out of 16) of *Tnfrsf11a*$^{75dup27/75dup27}$ mice died by 4 weeks of age compared to 0 % (0 out of 16) of wild type (WT) littermates. All *Tnfrsf11a*$^{75dup27/75dup27}$ mice became progressively unwell with age due to the severe osteopetrosis phenotype and they had to be culled by the age of 4 months. None of the *Tnfrsf11a*$^{75dup27/75dup27}$ mice had incisors by the time of culling. Radiographic analysis of these mice showed metaphyseal widening and sclerosis of the tibia and femur characteristic of osteopetrosis (Figure 1). The osteopetrosis was confirmed by MicroCT which also showed metaphyseal widening and thinning of the cortex (Figure 2). This phenotype was fully penetrant and affected all 16 mice analyzed. Detailed MicroCT analysis showed that *Tnfrsf11a*$^{75dup27/75dup27}$ mice had significantly higher BV/TV, trabecular number and trabecular thickness compared to WT whereas the trabecular separation was significantly lower than WT. (Figure 2). The trabecular area and peripheral circumference of tibiae were also significantly higher in homozygous mice. Histological analysis of Safranin-O and Fast Green stained sections showed expansion of the growth plate and the bone marrow cavity was filled with mineralized cartilage. No osteoclasts were detected upon TRAcP staining of bone sections from homozygous animals (Figure 2). In keeping with these observations, bone marrow-derived macrophages from *Tnfrsf11a*$^{75dup27/75dup27}$ mice failed to form osteoclasts *in vitro* in response to RANKL and M-CSF (Figure 2H).

*Phenotype of heterozygous Tnfrsf11a*$^{75dup27/-}$ *mice.*

Heterozygous *Tnfrsf11a*$^{75dup27/-}$ mice were viable and fertile, had normal survival and had a body size similar to wild type littermates. Analysis by X-ray showed no major differences between heterozygous and WT but some animals (3 out of 18) aged between 12-15 months showed osteolytic lesions in the tibia (Figure 1). MicroCT analysis of female 4-month old mice showed normal trabecular bone density and structure (Supplementary Table S2) with no evidence of osteolytic bone lesions. Consistent with the MicroCT results, histomorphometry of 4 month-old animals also showed no differences in bone density between WT and *Tnfrsf11a*$^{75dup27/-}$ animals (Supplementary Table S3). There was a trend for reduced Oc.S/BS and Oc.N/BS in heterozygous animals compared to WT but this was not statistically significant. Analysis of 4-month old male mice revealed similar results to those from female mice (data not shown).

We went on to analyze bone density and architecture by microCT of 12- and 15-month-old mice. We found that trabecular bone volume/tissue volume (BV/TV), trabecular thickness (Tb.Th), and trabecular number (Tb.N) were significantly higher in 12-month old *Tnfrsf11a*$^{75dup27/-}$ mice compared to WT (Figure 3). Additionally, trabecular separation (Tb.Sp) was significantly lower in *Tnfrsf11a*$^{75dup27/-}$ mice compared to WT. There was a trend for larger cortical thickens (Cort.Th) in *Tnfrsf11a*$^{75dup27/-}$ mice but this was not statistically significant (Figure 3). We observed larger peripheral circumference in *Tnfrsf11a*$^{75dup27/-}$ mice compared to WT indicating bone enlargement (Figure 3B). However, analysis of the skull bone showed no significant differences in morphology, width, length or height between Het and WT mice (Figure 3C and D).

We then assessed the mice for the presence of bone lesions by analysis of MicroCT images of the hind limbs. Results from 12-month-old mice showed lytic lesions at the proximal tibia and distal femur close to the growth plate and at both lower femoral condyles in *Tnfrsf11a*$^{75dup27/-}$ mice (Figure 4A). These lesions were similar to those previously reported in other mouse models of Paget's disease [12-14]. Most 12-month old heterozygous animals (7 out of 8) showed lesions similar to those shown in Figure 4A but by 15 months all (10 out of 10) *Tnfrsf11a*$^{75dup27/-}$ mice had developed lesions. However, some animals showed lesions in one limb only (2 out of 8 by 12 months and 2 out of 10 by 15-months) reminiscent of the focal nature of PDB. Analysis of bone lesion severity score showed a significantly higher score in heterozygous animals compared to WT (Figure 4B). The severity score was found to increase with age as 15-month-old animals had significantly higher score than 12-month-old animals ($P=0.005$).

A small number of heterozygous animals (3 out of 18) developed larger focal lesions in the tibial shaft of one limb as shown in Figure 4E and F. Histological analysis of these lesions revealed disorganized bone structure with a large number of osteoclasts in the area affected by the lesion ($74.5 \pm 7.8$ OC/mm$^2$) compared to the WT ($5.9 \pm 4.8$; $P= 4 \times 10^{-7}$; Figure 4E-F). Similarly, osteoblast numbers were higher in the lesion area ($147.1 \pm 8.8$ OB/mm$^2$) compared to WT ($21.6 \pm 3.9$; $P=5 \times 10^{-9}$).

Osteoclasts cultured from bone marrow cells of heterozygous *Tnfrsf11a*$^{75dup27/-}$ mice were fewer in number and had a smaller number of nuclei than those formed from wild type littermates (Figure 5A-B). They also appear to have a denser TRAcP staining compared to the WT osteoclasts. The percentage of larger osteoclasts (more than 5 nuclei) was decreased in cultures from *Tnfrsf11a*$^{75dup27/-}$ mice compared to wild type at both 100 and 200 ng/mL (Figure

5C). Analysis of osteoclast survival following withdrawal of RANKL showed that the percentage of surviving osteoclasts was significantly higher in the *Tnfrsf11a*$^{75dup27/-}$ cultures compared to wild type at all time points analyzed (Figure 5D).

*Effect of Tnfrsf11a*$^{75dup27/-}$ *mutation on NF-kB signaling in vitro*

In order to investigate the signaling mechanisms underlying the *in vitro* results for the *Tnfrsf11a*$^{75dup27/-}$ model, we analyzed ERK, IκB and p38 MAPK, c-Fos, and NF-κB pathways in MCSF-dependent macrophages in response to RANKL. We found no difference in ERK phosphorylation at baseline but following RANKL stimulation, there was an increased phosphorylation of ERK in osteoclasts cultured from *Tnfrsf11a*$^{75dup27/-}$ mice compared to WT and by 30 minutes, the levels of pERK in *Tnfrsf11a*$^{75dup27/-}$ mice were significantly higher than WT (Figure 6). However, IκB phosphorylation was significantly reduced in *Tnfrsf11a*$^{75dup27/-}$ osteoclasts after 10-15 min stimulation with RANKL compared with WT. Levels of phosphorylated p38 were greatly reduced in osteoclasts cultured from *Tnfrsf11a*$^{75dup27/-}$ mice compared to wild type, such that the mutant osteoclasts showed attenuated responses to RANKL. Analysis of c-Fos showed a significant increase in its level in mutant osteoclast precursor cells compared to WT but after RANKL stimulation, c-Fos levels were comparable to WT (Fig 6C). To assess NF-κB activity during osteoclast differentiation, we used a NF-κB luciferase reporter assay and found decreased NF-κB activity in the *Tnfrsf11a*$^{75dup27/-}$ at all stages during osteoclast differentiation compared with WT (Figure 6 E). However, when RANKL was withdrawn, NF-κB activity was higher in *Tnfrsf11a*$^{75dup27/-}$ cells, compared with wild type (Figure 6F).

We then assessed the effect of *Tnfrsf11a*$^{75dup27/-}$ mutation on serum levels of RANKL and biochemical markers of bone turnover in 4-month-old mice. We found no difference in serum levels of P1NP or CTX-I between *Tnfrsf11a*$^{75dup27/-}$ and WT but serum levels of RANKL were significantly lower in the mutant mice compared to WT (Figure 7).

*Zoledronic acid prevents development of osteolytic lesions in heterozygous Tnfrsf11a*$^{75dup27/-}$ *mice*

Administration of zoledronic acid between 4 and 12 months of age completely prevented the development of osteolytic lesions in heterozygous *Tnfrsf11a*$^{75dup27/-}$ mice whereas multiple lesions developed in the group receiving vehicle to a similar extent as in untreated heterozygous

mice (Figure 8). No obvious adverse effects were detected in mice which received zoledronic acid or PBS.

**Discussion**

Early onset Paget's disease of bone is a rare condition caused by a heterozygote duplication of 9 amino acids in the signal peptide of the RANK protein due a 27bp duplication in exon 1 of *TNFRSF11A*. It shares some of the clinical features of classical PDB, but has an earlier age of onset, and is characterized by early onset deafness, premature tooth loss, and prominent involvement of the mandible and maxilla [(1)]. Early functional studies of the *TNFRSF11A* 27bp duplication showed that when constructs containing the mutant allele were over-expressed in HEK293 cells, there was an evidence of increased constitutive NF-κB activation in promoter-reporter assays when compared with wild type [(3)]. These observations were confirmed by Crockett and colleagues but when the 75dup27 allele and the related 84dup18 and 84dup15 alleles were stably expressed as a single copy in HEK 293 cells, there was no evidence of increased NF-κB activation. Furthermore, Crockett et al [(5)] demonstrated that cells stably expressing these three mutant alleles failed to respond to RANKL stimulation and that the mutant proteins failed to translocate to the cell surface, but instead accumulated in organized smooth endoplasmic reticulum (OSER) - like structures. The overall conclusion from Crockett's experiments were that the insertion mutations were loss-of-function variants that result in a failure to respond to RANKL *in vitro*.

The experiments described here confirm that the 75dup27 mutation is a loss-of function variant which fails to respond to RANKL. Reflecting this fact, mice homozygous for the 75dup27 variant had features of osteopetrosis *in vivo* which include metaphyseal widening and sclerosis of the tibia and femur and total absence of osteoclasts in histological sections. Furthermore, the bone marrow cavity was filled with mineralized cartilage which is confirmed by significantly higher BV/TV, Tb.N, Tb.Th and Trabecular area. Consistent with this, bone marrow cells from these mice failed to differentiate into osteoclasts in response to MCSF and RANKL stimulation, a phenotype that is similar to that of mice with targeted inactivation of RANK [(15)]. In contrast, *Tnfrsf11a*$^{75dup27/-}$ mice appeared normal at a young adult age (4 month) but analysis by histomorphometry showed a trend for lower OC.N/BS compared to WT, nonetheless trabecular bone indices analyzed by micro CT showed no significant differences between heterozygous and WT mice. Additionally, the serum levels of bone turnover markers P1NP

and CTX-I were comparable to those observed in age-matched WT mice, however serum levels of RANKL were significantly reduced in heterozygous mice.

When heterozygous mice were analyzed at an older age (12 months), they exhibited higher BV/TV, Tb.N, and Tb.Th and there was an evidence of bone enlargement as evident from larger peripheral circumference in hind limbs of heterozygous mice compared to WT. However, the skull bones from these mice were normal with no significant differences to WT.

We also found that heterozygous mice developed focal osteolytic lesions in the lower limbs with increasing age, consistent with the phenotype observed in humans with this mutation. At the age of 12 months, most animals developed osteolytic lesions at the proximal tibia and distal femur close to the growth plate and the lesion severity was found to increase with age.

To identify the molecular mechanisms involved in the maintenance of the osteoclast activity, we evaluated a number of molecular targets from MAPK and NF-κB pathways, associated with osteoclastogenesis and osteoclast function. We found that cells cultured from mice heterozygous for the 75dup27 mutation showed a decreased IκB and p38 phosphorylation, compared to wild type controls. A decrease in the expression of the active form of IκB (pIκB) has been associated with reduced osteoclastogenesis (reviewed in [16]). In the same line, p38, a member of the MAPK family, plays a role in the differentiation of bone marrow cells into osteoclasts [17]. Therefore, the reduction in osteoclastogenesis found in the *Tnfrsf11a*$^{75dup27/-}$ model could be caused by a decrease in IκB and p38 activation. We also detected an increase of ERK phosphorylation in the heterozygotes compared with WT. ERK is involved in a number of processes in osteoclasts, including survival, proliferation, cell polarity, and differentiation, among others [18]. Increasing ERK phosphorylation could be associated to the increased osteoclast survival found in our model, since the increase in pERK was sustained for longer time and became significant at 30 min post RANKL activation. Additionally, basal c-Fos expression was higher in osteoclast precursors of heterozygous animals which may also partially explain the increased survival of osteoclasts.

Analysis of NF-κB activity during osteoclast differentiation in the *Tnfrsf11a*$^{75dup27/-}$ mice showed that RANKL-induced NF-κB activation was reduced in heterozygous animals compared to WT, consistent with our western blot results and with previous *in vitro* studies [5]. However, after withdrawal of RANKL, the NF-κB expression is sustained and increased compared with wild type controls. NF-κB is important for osteoclast function and survival (reviewed in [19]), and its continuous activation to trigger RANK pathway in absence of the

ligand could be associated with increased osteoclast survival, ultimately leading to the bone lesions reminiscent of Paget's disease that were found in the *Tnfrsf11a*$^{75dup27/-}$ mice *in vivo*.

Previous *in vitro* studies have reported a continuous activation of the RANK pathway caused by mutations in the signal peptide of RANK leading to a hyperactivity of the osteoclasts, but the mechanism involved was unclear [3]. It has been demonstrated that the 75dup27 and other mutations in the signal peptide of RANK impair cleavage of the signal peptide and prevent the RANK protein migrating to the plasma membrane [20,21]. Instead the mutant protein has been shown to accumulate in OSER-like structures in endoplasmic reticulum [22]. The mechanism by which the abnormal protein stimulates osteoclast survival is unknown but a possibility would be by triggering the unfolded protein response (UPR) which is known to cause activation of NF-κB signaling [23]. Furthermore, accumulation of unfolded proteins and/or a decreased capacity to degrade unfolded proteins with age [24], could contribute to increased penetrance of the Paget's disease-like phenotype with age that we observed in *Tnfrsf11a*$^{75dup27/-}$ mice.

In addition to clarifying the mechanisms of action by which these mutations cause osteolytic lesions, the present experiment has shown that when administered early in life, zoledronic acid can prevent the development of lesions at older age. While bisphosphonates have not been shown to reverse bone deformity, improve mobility or prevent deafness and tooth loss in patients with EoPDB [2], it should be noted that the treatment was administered at a late stage in the disease process. Our data suggest that if prophylactic therapy was given at an early stage, it may be possible to prevent or inhibit the progression of bone disease in this severe and disabling disorder.

**Acknowledgments**

This work was funded in part by a grant from the Medical Research Council to OMEA and SHR (G0800933/87390), a grant from the Wellcome Trust to SHR (060829/Z/00Z) a consolidator grant from the European Research Council to OMEA (311723-GENEPAD) and an advanced investigator grant from the European Research Council to SHR (787270 - Paget-Advance).

We thank Marcin Kruk, Huilin Jin, Euphemie Landao, Gemma Charlesworth, Catherine Sperinck and Amanda Prior for their assistance with MicroCT scanning and histology and Asim Azfer for assistance with western blotting.

**Author Roles**

SHR and OMEA designed the study. NA, SW, and LR performed the experiments. NA, OMEA, SW, and RvH analyzed the data. NA drafted the manuscript. OMEA and SHR revised the manuscript. OMEA and SHR supervised the project. All authors contributed to critically review the article and approved the final manuscript.



**References**


1. Nakatsuka K, Nishizawa Y, Ralston SH. Phenotypic characterization of early onset Paget's disease of bone caused by a 27-bp duplication in the TNFRSF11A gene. J Bone Miner Res. Aug 2003;18(8):1381-5. Epub 2003/08/22.
2. Riches PL, Imanishi Y, Nakatsuka K, Ralston SH. Clinical and biochemical response of TNFRSF11A-mediated early-onset familial Paget disease to bisphosphonate therapy. Calcif Tissue Int. Oct 2008;83(4):272-5. Epub 2008/10/07.
3. Hughes AE, Ralston SH, Marken J, Bell C, MacPherson H, Wallace RG, et al. Mutations in TNFRSF11A, affecting the signal peptide of RANK, cause familial expansile osteolysis. Nat Genet. Jan 2000;24(1):45-8. Epub 1999/12/30.
4. Ralston SH, Taylor JP. Rare Inherited forms of Paget's Disease and Related Syndromes. Calcif Tissue Int. May 2019;104(5):501-16. Epub 2019/02/14.
5. Crockett JC, Mellis DJ, Shennan KI, Duthie A, Greenhorn J, Wilkinson DI, et al. Signal peptide mutations in RANK prevent downstream activation of NF-kappaB. J Bone Miner Res. Aug 2011;26(8):1926-38. Epub 2011/04/08.
6. von Heijne G. Signal sequences. The limits of variation. J Mol Biol. Jul 5 1985;184(1):99-105. Epub 1985/07/05.
7. Helfrich MH, Hocking LJ. Genetics and aetiology of Pagetic disorders of bone. Arch Biochem Biophys. May 15 2008;473(2):172-82. Epub 2008/03/25.
8. Itzstein C, van 't Hof RJ. Osteoclast formation in mouse co-cultures. Methods Mol Biol. 2012;816:177-86. Epub 2011/12/02.
9. van 't Hof RJ, Dall'Ara E. Analysis of Bone Architecture in Rodents Using Micro-Computed Tomography. Methods Mol Biol. 2019;1914:507-31. Epub 2019/02/08.
10. van 't Hof RJ, Rose L, Bassonga E, Daroszewska A. Open source software for semi-automated histomorphometry of bone resorption and formation parameters. Bone. Jun 2017;99:69-79. Epub 2017/04/04.
11. Dempster DW, Compston JE, Drezner MK, Glorieux FH, Kanis JA, Malluche H, et al. Standardized nomenclature, symbols, and units for bone histomorphometry: a 2012 update of the report of the ASBMR Histomorphometry Nomenclature Committee. J Bone Miner Res. Jan 2013;28(1):2-17. Epub 2012/12/01.
12. Obaid R, Wani SE, Azfer A, Hurd T, Jones R, Cohen P, et al. Optineurin Negatively Regulates Osteoclast Differentiation by Modulating NF-kappaB and Interferon Signaling: Implications for Paget's Disease. Cell Rep. Nov 10 2015;13(6):1096-102. Epub 2015/11/04.
13. Daroszewska A, van 't Hof RJ, Rojas JA, Layfield R, Landao-Basonga E, Rose L, et al. A point mutation in the ubiquitin-associated domain of SQSMT1 is sufficient to cause a Paget's disease-like disorder in mice. Hum Mol Genet. Jul 15 2011;20(14):2734-44. Epub 2011/04/26.
14. Daroszewska A, Rose L, Sarsam N, Charlesworth G, Prior A, Rose K, et al. Zoledronic acid prevents pagetic-like lesions and accelerated bone loss in the p62(P394L) mouse model of Paget's disease. Dis Model Mech. Aug 23 2018;11(9). Epub 2018/08/30.

15. Dougall WC, Glaccum M, Charrier K, Rohrbach K, Brasel K, De Smedt T, et al. RANK is essential for osteoclast and lymph node development. Genes Dev. Sep 15 1999;13(18):2412-24. Epub 1999/09/29.
16. Boyce BF, Xiu Y, Li J, Xing L, Yao Z. NF-kappaB-Mediated Regulation of Osteoclastogenesis. Endocrinol Metab (Seoul). Mar 27 2015;30(1):35-44. Epub 2015/04/02.
17. Matsumoto M, Sudo T, Saito T, Osada H, Tsujimoto M. Involvement of p38 mitogen-activated protein kinase signaling pathway in osteoclastogenesis mediated by receptor activator of NF-kappa B ligand (RANKL). J Biol Chem. Oct 6 2000;275(40):31155-61. Epub 2000/06/22.
18. Nakamura H, Hirata A, Tsuji T, Yamamoto T. Role of osteoclast extracellular signal-regulated kinase (ERK) in cell survival and maintenance of cell polarity. J Bone Miner Res. Jul 2003;18(7):1198-205. Epub 2003/07/12.
19. Novack DV. Role of NF-kappaB in the skeleton. Cell Res. Jan 2011;21(1):169-82. Epub 2010/11/17.
20. Crockett JC, Mellis DJ, Scott DI, Helfrich MH. New knowledge on critical osteoclast formation and activation pathways from study of rare genetic diseases of osteoclasts: focus on the RANK/RANKL axis. Osteoporos Int. Jan 2011;22(1):1-20. Epub 2010/05/12.
21. Nilsson I, Whitley P, von Heijne G. The COOH-terminal ends of internal signal and signal-anchor sequences are positioned differently in the ER translocase. J Cell Biol. Sep 1994;126(5):1127-32. Epub 1994/09/01.
22. Snapp EL, Hegde RS, Francolini M, Lombardo F, Colombo S, Pedrazzini E, et al. Formation of stacked ER cisternae by low affinity protein interactions. J Cell Biol. Oct 27 2003;163(2):257-69. Epub 2003/10/29.
23. Deng J, Lu PD, Zhang Y, Scheuner D, Kaufman RJ, Sonenberg N, et al. Translational repression mediates activation of nuclear factor kappa B by phosphorylated translation initiation factor 2. Mol Cell Biol. Dec 2004;24(23):10161-8. Epub 2004/11/16.
24. Santra M, Dill KA, de Graff AMR. Proteostasis collapse is a driver of cell aging and death. Proc Natl Acad Sci U S A. Oct 29 2019;116(44):22173-8. Epub 2019/10/18.

**Figure Legends**

**Figure 1. X-ray images of mice with *Tnfrsf11a* 75dup27 mutation. Upper row:** wild type (WT; 15 month female), *Tnfrsf11a*$^{75dup27/-}$ (15 month, female) and *Tnfrsf11a*$^{75dup27/75dup27}$ (2.5 month female) mice. **lower row:** X-ray amplification of the knee joint showing part of the femur, tibia and fibula. Arrows indicate bone lesions in heterozygote animals. Homozygote animals show metaphyseal widening and sclerosis of the tibia and femur characteristic of osteopetrosis.

**Figure 2. Analysis of bone phenotype in 4-month-old *Tnfrsf11a*$^{75dup27/75dup27}$ mice**. (**A, D**) Bone sections from female WT (**A**) and *Tnfrsf11a*$^{75dup27/75dup27}$ (**D**) mice stained with Safranin O, to visualize cartilage matrix (red color), and Fast green as a counterstain. The marked section of the image is shown at higher magnification in the panel below. (**B, E**) Representative 3D MicroCT images of tibia from WT (**B**) and *Tnfrsf11a*$^{75dup27/75dup27}$ (**E**) mice. (**C, F**) Bone sections from WT (**C**) and *Tnfrsf11a*$^{75dup27/75dup27}$ (**F**) mice stained with TRAcP, to visualize osteoclasts (indicated by arrows), and Aniline Blue as a counterstain. (**G**) MicroCT analysis of bone structure showing comparison of bone volume/tissue volume (BV/TV), trabecular thickness (Tb.Th), trabecular separation (Tb.Sp), trabecular number (Tb.N), trabecular area (T.Ar) and peripheral circumference (Per.Circ) between WT (*n*=6) and *Tnfrsf11a*$^{75dup27/75dup27}$ (HOM; *n*=6) mice. **(H)** Representative images of TRAcP stained osteoclast cultures from *Tnfrsf11a*$^{75dup27/75dup27}$ compared to WT, after stimulation of bone marrow derived macrophages with MCSF and different concentrations of RANKL for 5 days. Results are representative of three independent biological replicates.

**Figure 3. Analysis of bone phenotype in 12-month-old *Tnfrsf11a*$^{75dup27/-}$ mice by MicroCT**. (**A**) Representative 3D MicroCT images of distal femur from WT and Heterozygous mice (Het). (**B**) Comparison of cortical thickness (Cort.Th), peripheral circumference (Per.Circ), bone volume/tissue volume (BV/TV), trabecular thickness (Tb.Th), trabecular separation (Tb.Sp) and trabecular number (Tb.N) between WT (n=6) and Het (n=7) female mice. (**C**) Representative 3D MicroCT images of the skull from WT and Het mice. (**D**) Comparison of skull bone width, height and length between WT (n=6) and Het (n=6) female mice.

**Figure 4. Bone lesions in *Tnfrsf11a*$^{75dup27/-}$ mice**. (**A**) Representative 3D MicroCT images of proximal femur from female WT and *Tnfrsf11a*$^{75dup27/-}$ (Het) mice. The most common sites for

lesions were distal femur (indicated by arrows) and proximal tibia (not shown). **(B)** Box and whisker plot showing lesion score in 12-month and 15-month old female Het animals compared to WT; *n* indicates the number of animals per group. (**C,E**) Representative 3D MicroCT images of tibia from a 15-month old female WT (**C**) compared to Het (**E**) mouse showing the development of severe bone lesions (black arrows). The panels to the right represent a longitudinal and axial view, respectively, showing the lesions detected in the tibial cortex of Het mice (indicated by red arrows and oval markings). (**D,F**) Histological sections of the regions indicated by red oval markings from WT **(D)** and Het (**F**) mice. Bone sections were stained with TRAcP, to visualize osteoclasts, and Aniline Blue as a counterstain. The panel to the right represents a higher magnification image. Scale bars = 100μm unless stated otherwise.

**Figure 5. Osteoclast cultures from 4-month-old** *Tnfrsf11a*$^{75dup27/-}$ . (**A)** Representative images of TRAcP stained osteoclast cultures from *Tnfrsf11a*$^{75dup27/-}$ (Het) compared to WT after stimulation with MCSF and different concentrations of RANKL. Scale bar = 100 μm (**B)** Quantification of the number of osteoclasts (OC) formed after RANKL stimulation in Het and WT mice. (**C)** Percentage of large osteoclast (> 5 nuclei) over total number of osteoclasts in Het and WT mice after RANKL stimulation. (**D)** Quantification of the percentage of osteoclast survival after RANKL withdrawal in Het and WT mice at the indicated time points. Results are representative of three independent biological replicates from female mice.

**Figure 6. Analysis of signaling pathways in 4-month-old** *Tnfrsf11a*$^{75dup27/-}$ **mice**. (**A)** Western blot images of pERK; pIκB; and pp38 in primary osteoclast cultures from *Tnfrsf11a*$^{75dup27/-}$ (Het) compared to WT mice at the indicated time points of RANKL stimulation. (**B**) Band intensity analysis of pERK; pIκB; and pp38. (**C**) Western blot images of cFos in primary osteoclast cultures from Het compared to WT mice after RANKL stimulation. The box plot to the right represents band intensity analysis of cFos. All western blot results are shown as a percentage of unstimulated WT (0 min) and were from 2-4 independent biological replicates. (**D**) Luciferase assay for NF-κB activation during osteoclast differentiation from bone marrow derived cells upon stimulation with RANKL in WT compared to Het. (**E)** RANKL withdrawal; luciferase assay for NF-κB activation in osteoclasts and up to 48 hours post RANKL withdrawal. Results are representative of three independent biological replicates.

**Figure 7. Serum levels of biochemical markers of bone turnover in 4-month-old RANK *Tnfrsf11a*$^{75dup27/-}$ mice.** (**A**) Serum levels of Procollagen Type I N-terminal propeptide (P1NP); (**B**) carboxy-terminal telopeptide cross-links (CTX-I); and (**C**) RANKL in WT (*n*=8) compared to *Tnfrsf11a*$^{75dup27/-}$ (Het; *n*=8) female mice.

**Figure 8. Effect of Zoledronic acid treatment on the development of bone lesions in RANK *Tnfrsf11a*$^{75dup27/-}$ mice.** Bone lesions in 15-month-old *Tnfrsf11a*$^{75dup27/-}$ female mice treated with zoledronic acid (*n*=8) or PBS (*n*=8). **(A)** Box and whisker plot showing lesion score. **(B**) Representative 3D MicroCT images of tibia and femur from heterozygous animals treated with PBS (Het-PBS) or zoledronic acid (Het-Zol). Arrows indicate observed bone lesions. No lesions were observed in the zoledronic acid group.

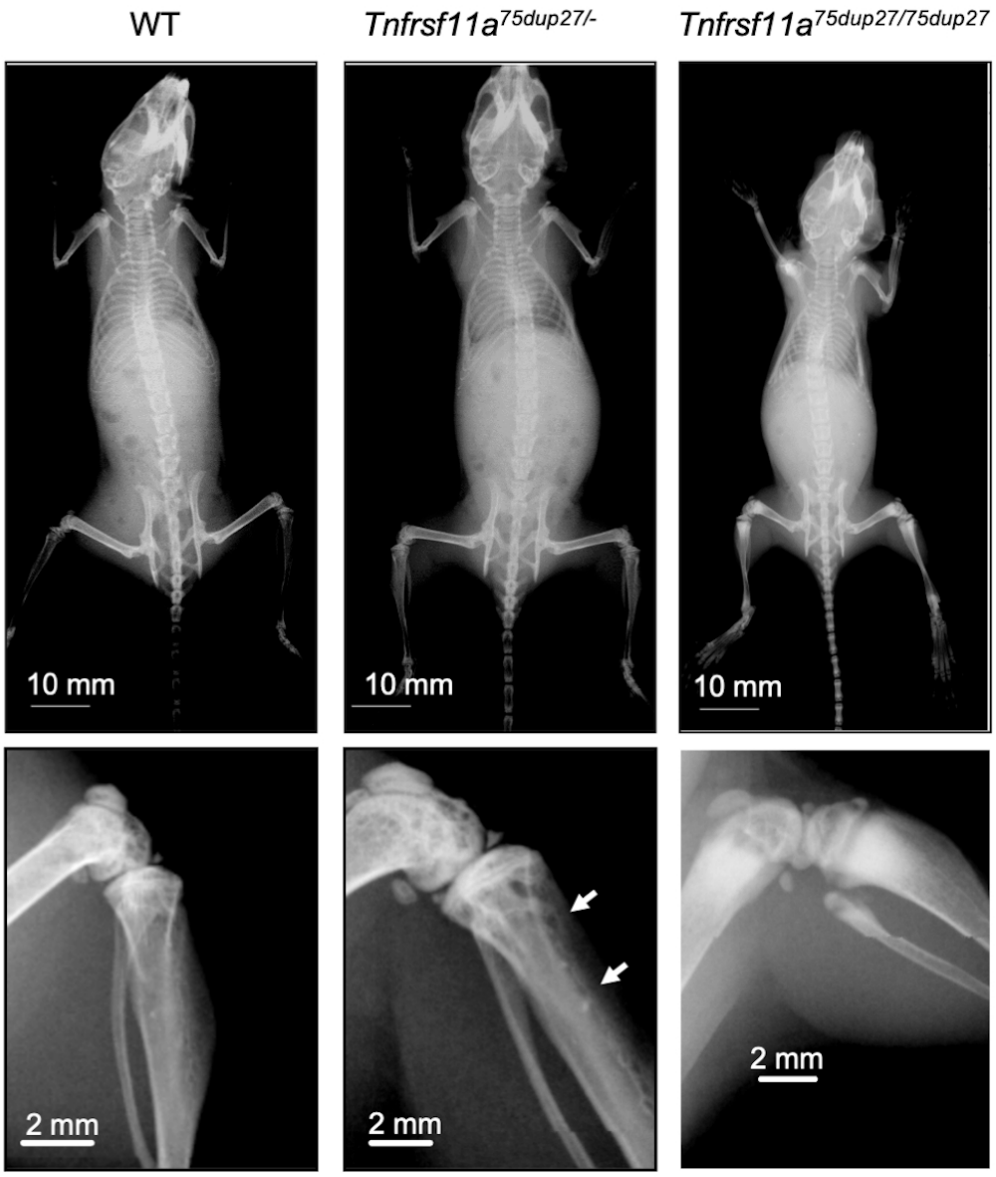


Fig.1

85x100mm (300 x 300 DPI)

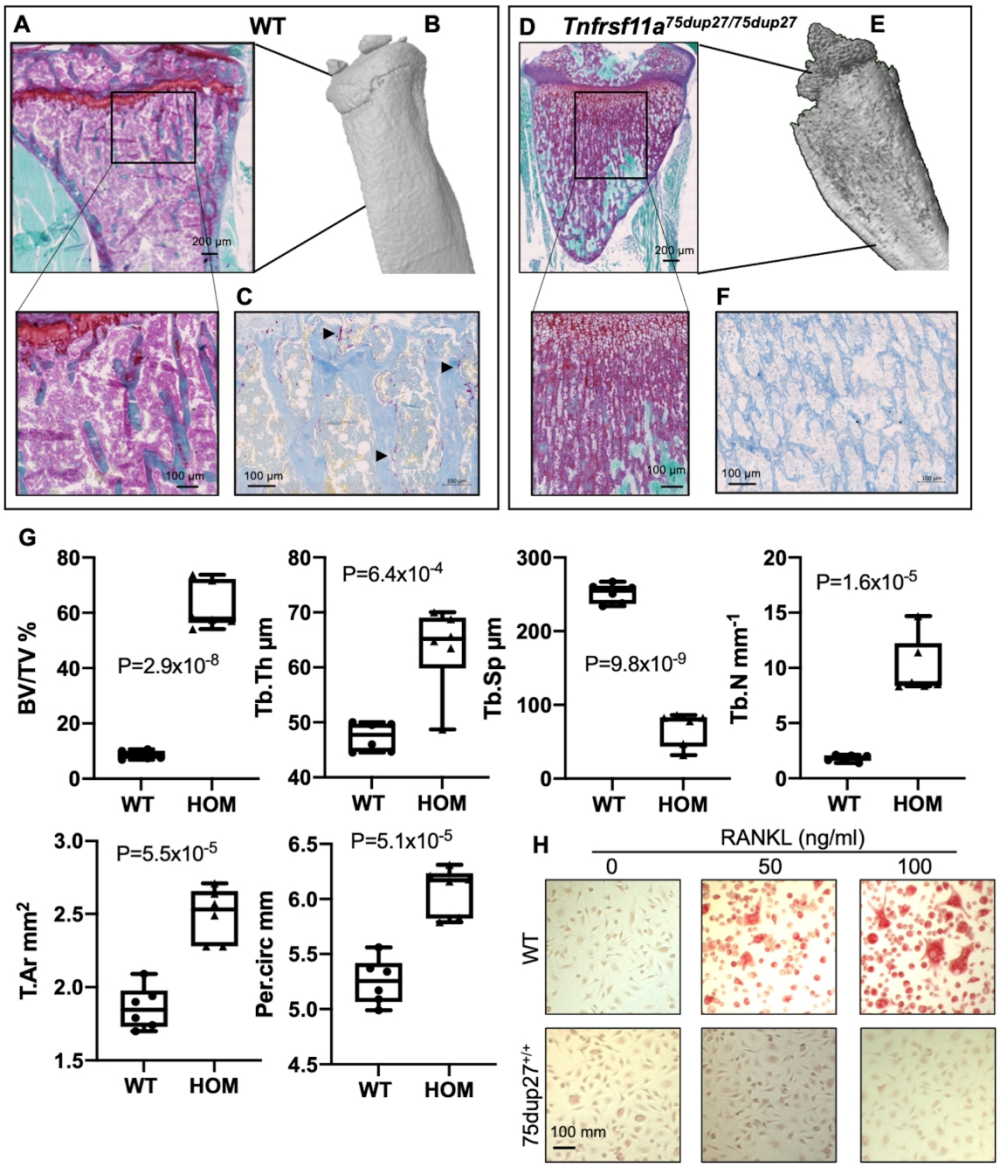


Fig.2

177x206mm (300 x 300 DPI)

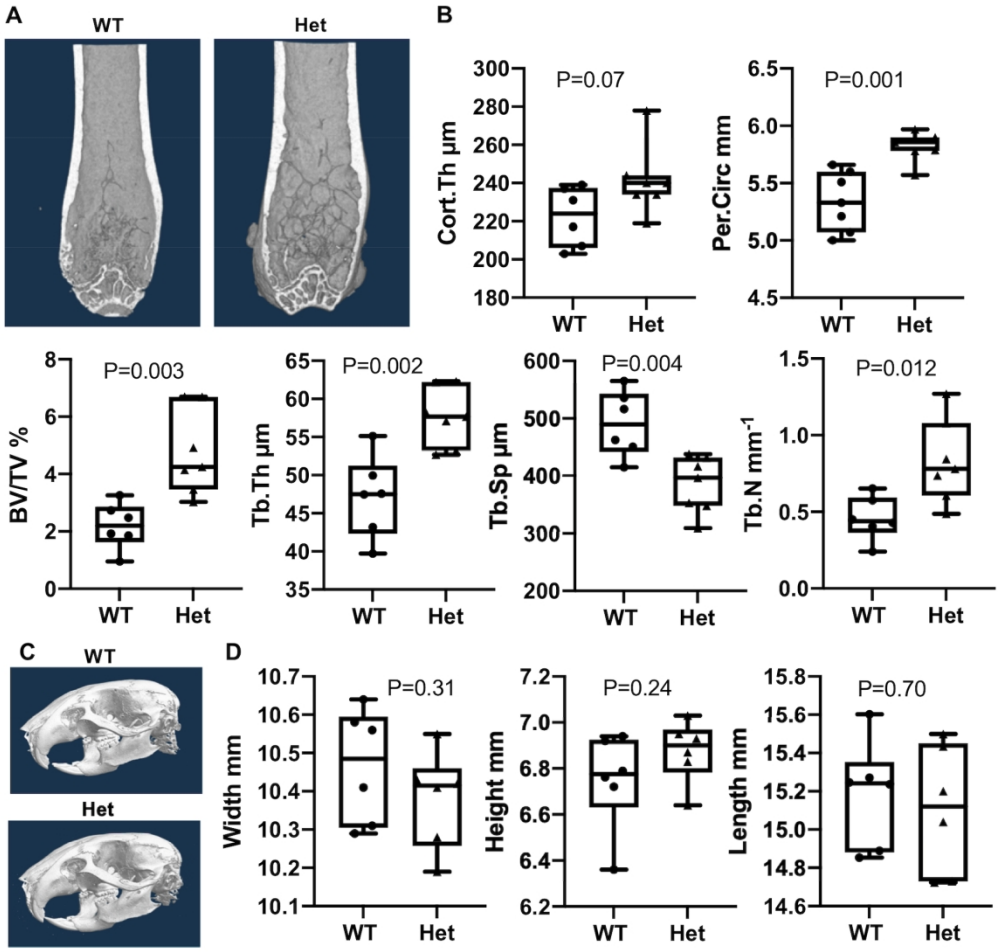


Fig.3

177x167mm (300 x 300 DPI)

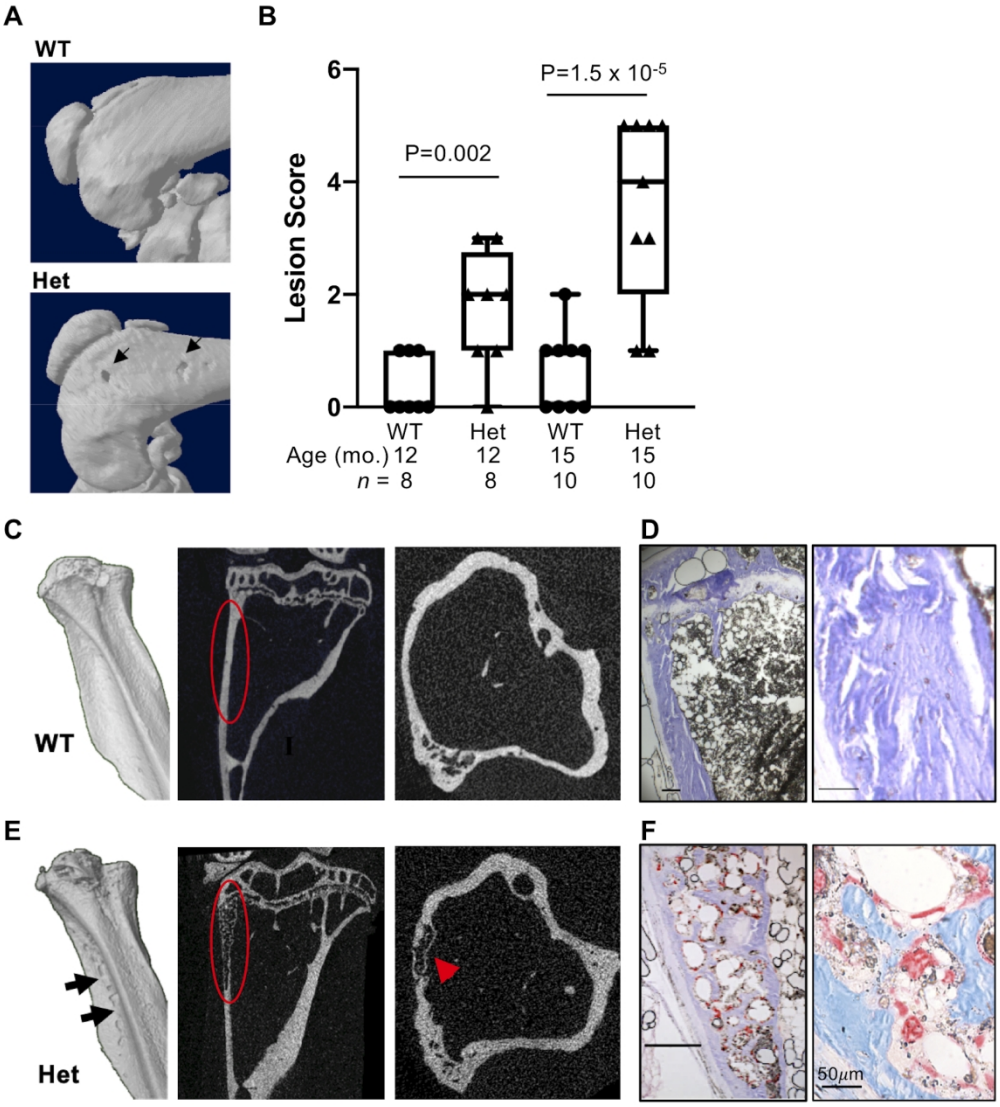


Fig.4

177x195mm (300 x 300 DPI)

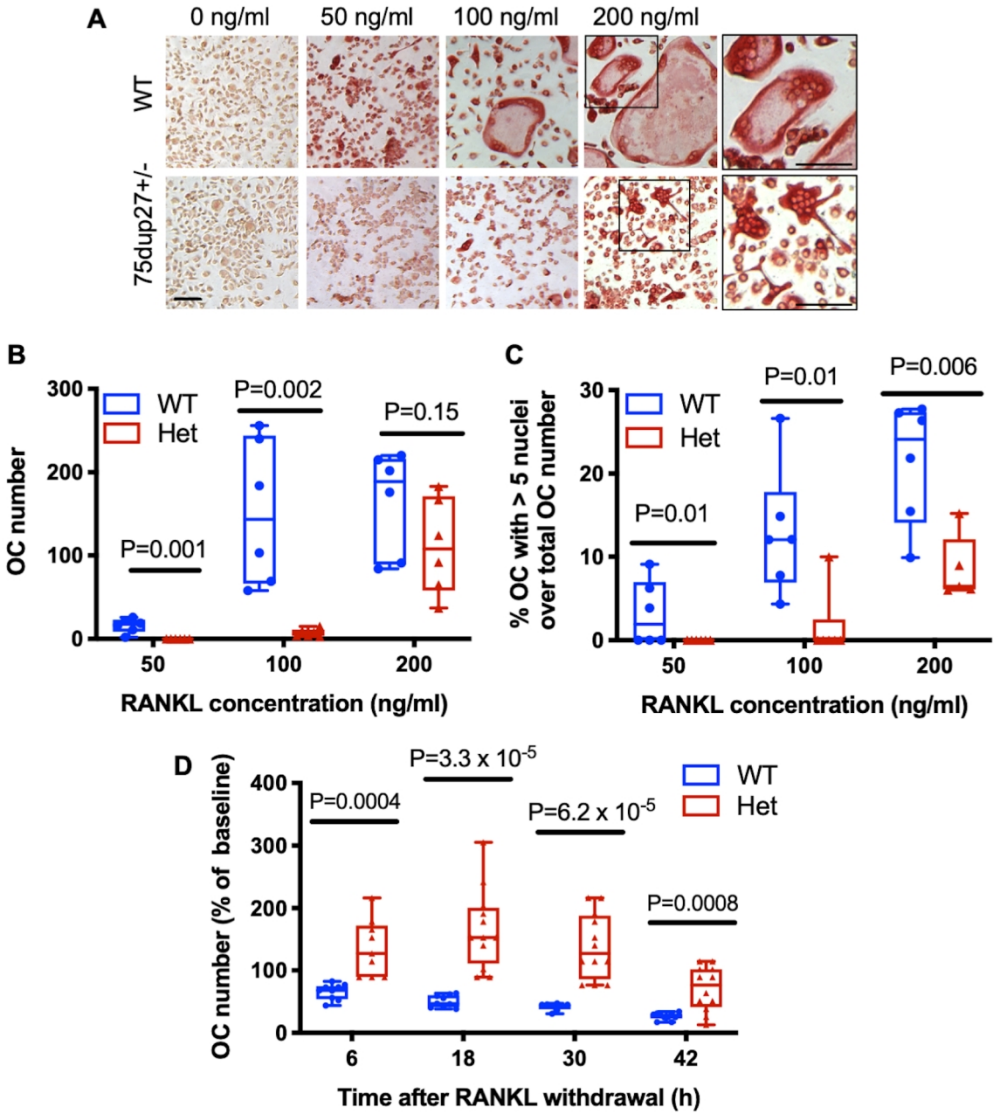


Fig.5

150x171mm (300 x 300 DPI)

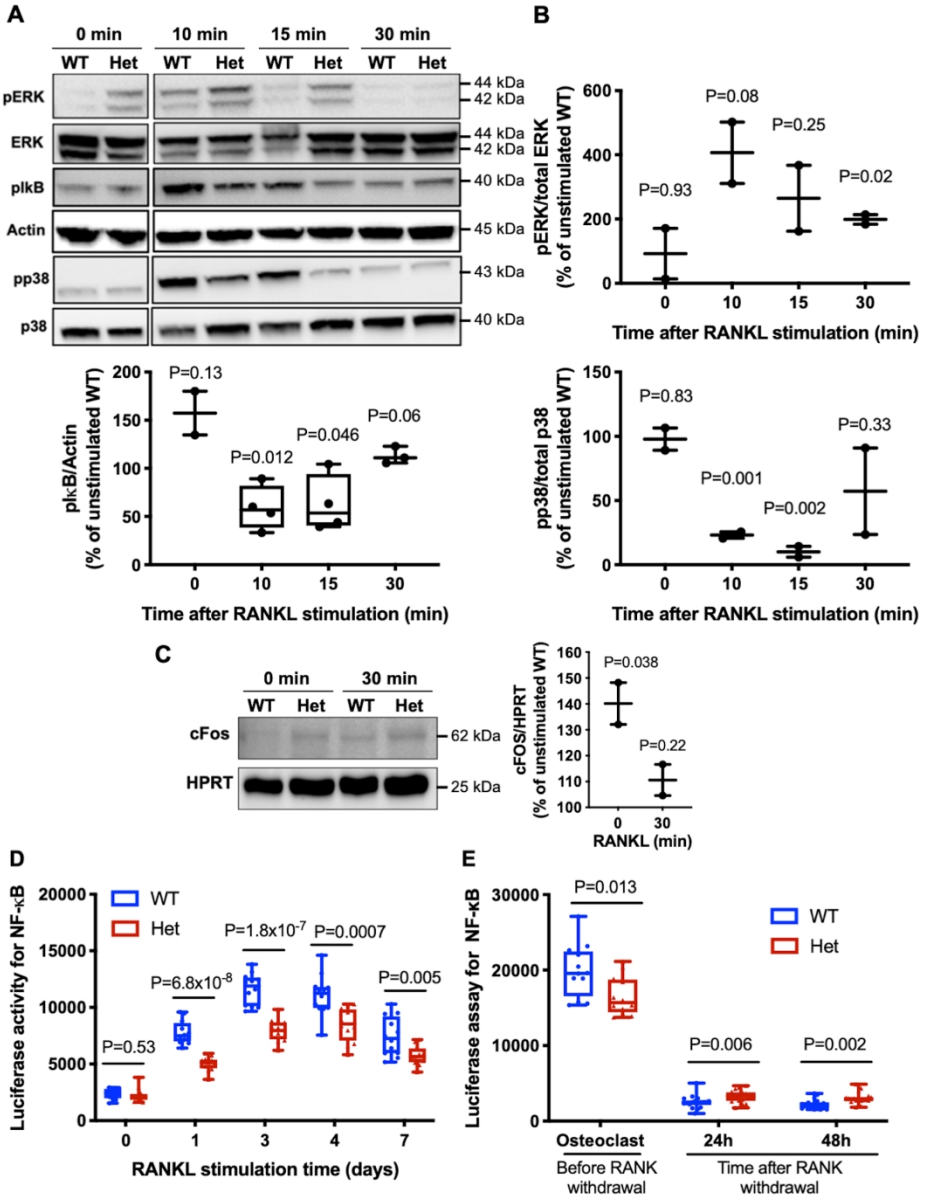


Fig.6

177x228mm (300 x 300 DPI)

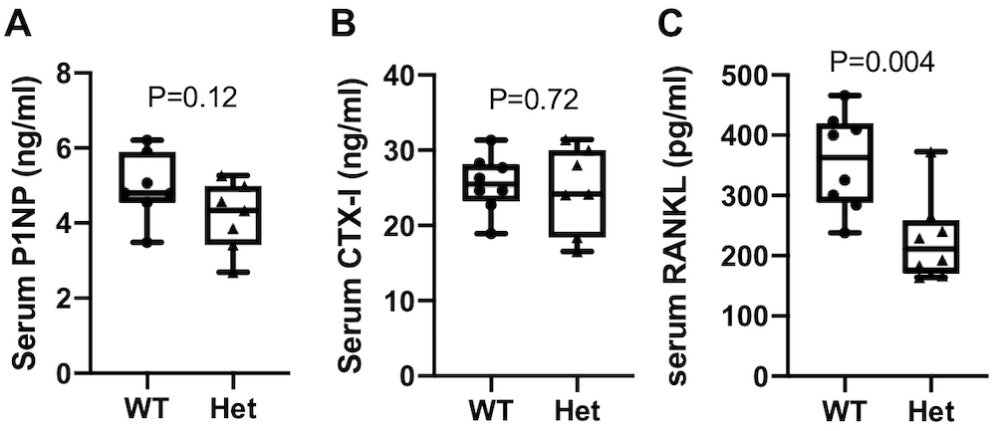


Fig.7

85x37mm (300 x 300 DPI)

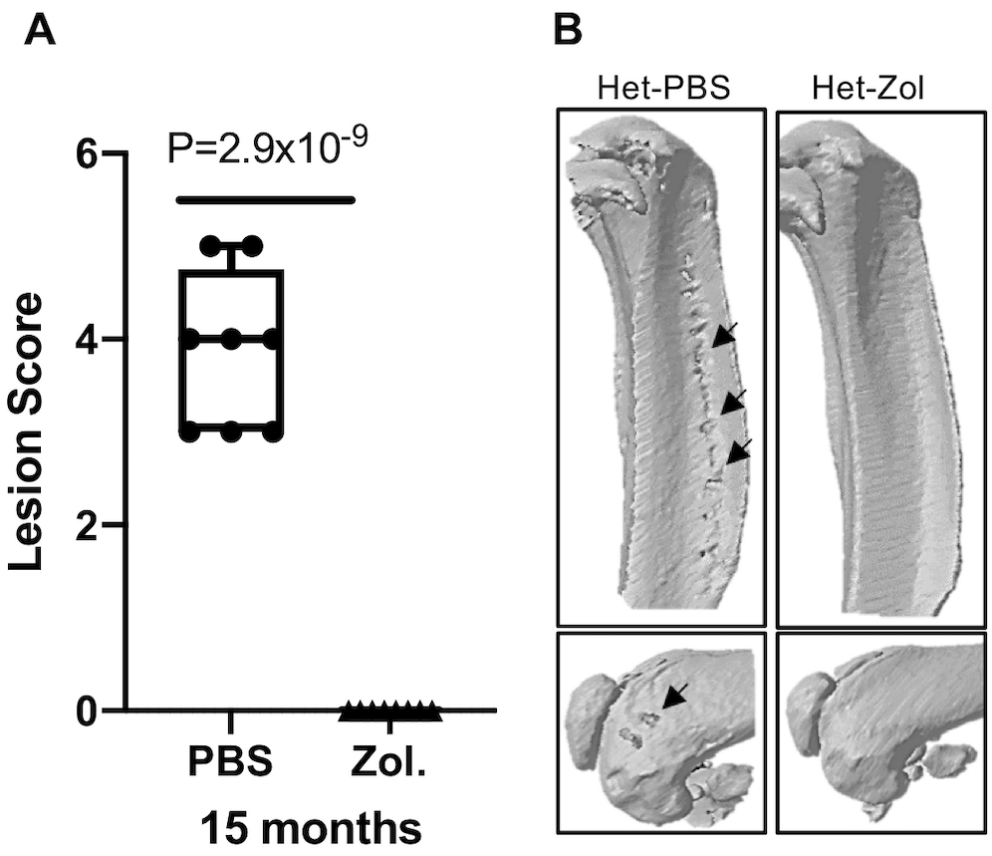


Fig.8

85x72mm (300 x 300 DPI)